JMEPEG (2011) 20:1068–1077
DOI: 10.1007/s11665-010-9728-8

1059-9495/$19.00

# Hot Corrosion Studies of Detonation-Gun-Sprayed NiCrAlY + 0.4 wt.% $CeO_2$ Coated Superalloys in Molten Salt Environment

*Subhash Kamal, R. Jayaganthan, and Satya Prakash*

*(Submitted January 31, 2010; in revised form June 15, 2010)*

**Rare earth oxide ($CeO_2$) has been incorporated in NiCrAlY alloy and hot corrosion resistance of detonation-gun-sprayed NiCrAlY + 0.4 wt.% $CeO_2$ coatings on superalloys, namely, superni 75, superni 718, and superfer 800H in molten 40% $Na_2SO_4$-60% $V_2O_5$ salt environment were investigated at 900 °C for 100 cycles. The coatings exhibited characteristic splat globular dendritic structure with diameter similar to the original powder particles. The weight change technique was used to establish corrosion kinetics. X-ray diffraction (XRD), field emission scanning electron microscopy/energy-dispersive analysis (FE-SEM/EDAX), and x-ray mapping techniques were used to analyze the corrosion products. Coated superfer 800H alloy showed the highest corrosion resistance among the examined superalloys. $CeO_2$ was found to be distributed in the coating along the splat boundaries, whereas Al streaks distributed non-uniformly. The main phases observed for the coated superalloys are oxides of Ni, Cr, Al, and spinels, which are suggested to be responsible for developing corrosion resistance.**

**Keywords** hot corrosion, microstructures, SEM, superalloys

## 1. Introduction

Superalloys find their largest application in the gas turbine industry, constituting over 50% of the gas turbine weight; these are preferred because of their superior mechanical strength, surface stability, creep and fatigue resistance (Ref 1). These superalloys are exposed to high temperature and tend to suffer from significant degradation due to corrosion during service (Ref 2, 3). In utility gas turbines, contaminants in the fuel and air can cause serious hot corrosion problems. A wide range of fuel is used in utility turbines (ranging from clean gas to crude oil) and these fuels contain sulfur, sodium, potassium, vanadium, and lead, as contaminants (Ref 4). The corrosion causing elements enter with the air ingested into the turbine inlet and with fuel. NaCl in the seawater react with the sulfur impurity in the fuel to form $Na_2SO_4$ within the engine (Ref 5), by the following reaction, which has been proposed by DeCrescente and Bornstein (Ref 6).

$$2NaCl + SO_3 + 1/2O_2 \rightarrow Na_2SO_4 + Cl_2 \quad \text{(Eq 1)}$$

Small amount of vanadium may be present in fuel oils, which on combustion forms $V_2O_5$. This may further reacts with $Na_2SO_4$ to form low melting sodium vanadates, this is highly corrosive in nature as reported by Sidhu et al. (Ref 7).

$$Na_2SO_4 + V_2O_5 \rightarrow (Na_2O) \cdot V_2O_5 + SO_3 \quad \text{(Eq 2)}$$

During operation, blades and vanes of gas turbines have to withstand both mechanical and thermal loadings as well as chemical attack by oxidation, which increases significantly with temperature. The base material (usually a Ni-base superalloy) provides the necessary mechanical properties and coatings provide protection against oxidation and corrosion (Ref 8).

Recent studies showed that the materials used for high temperature strength are highly susceptible to hot corrosion and the surface engineering plays a key role in effectively combating the hot corrosion and oxidation problems (Ref 9, 10). Increasing demands for the high performance superalloy make the surface coatings more favorable than ever, as they offer cost-effective ways to combat degradation resulting from mechanisms such as wear, oxidation, and corrosion (Ref 11, 12).

Overlay coatings are a family of corrosion resistant alloys specially designed for high temperature surface protection. They are often referred to as M-Cr-Al-Y coatings, where M is the alloy base metal (typically nickel, cobalt, or combination of these two), and the high chromium low aluminum M-Cr-Al-Y coatings typically resist low temperature hot corrosion (LTHC) attack, while lower chromium and higher aluminum contents are typically required for high temperature hot corrosion (HTHC) resistance (Ref 13). Detonation-gun (D-gun) spray coating process is a thermal spray process, which gives an extremely good adhesive strength, low porosity, and coating surfaces with compressive residual stress (Ref 14). Due to its low porosity and good adhesion, D-gun-sprayed coating can effectively decrease the inward diffusion of oxygen (Ref 11). Splat thickness of D-gun sprayed coating is less, as impact velocity is 2-3 times higher than that of the other thermal spray processes (Ref 15). Addition of 0.4 wt.% $CeO_2$ can considerably improve the properties of MCrAlY coating. Cerium is a surface-active element and thus reduces the surface tension and

**Subhash Kamal, R. Jayaganthan** and **Satya Prakash**, Department of Metallurgical and Materials Engineering, Indian Institute of Technology Roorkee, Roorkee 247667, India. Contact e-mail: rjayafmt@iitr.ernet.in.

the interfacial energy between the crystal nucleus and the melt during the process of solidification (Ref 16). Zhang and Li (Ref 17) have found that cerium improved the protective efficiency of the aluminide coating against dry sand erosion and corrosion in dilute NaCl and $H_2SO_4$ solution, respectively. In recent studies, it has been shown that the erosion resistance of aluminide coatings can be improved by rare earth elements, for example, yttrium improved the resistance of FeAlCr(Y) coatings to corrosion, corrosive erosion, and dry sand erosion, respectively (Ref 18). Seybolt (Ref 19) studied the role of rare earth additions on the hot corrosion behavior of various Ni-based alloys in liquid $Na_2SO_4$ in still air at 1000 °C, he has concluded that the rate of hot corrosion attack is diminished due to the influence of rare earth. Further, it was observed that rare earth addition in the form of oxides are very effective in minimizing the hot corrosion as it forms oxysulfides by combining with sulfur. Gitanjaly (Ref 20) has reported that superficial application of ceria on Fe- and Ni-based superalloys lead to the marked reduction in oxidation rate under aggressive environment of molten salt at 900 °C. She reported that presence of $CeO_2$ on the surface led to the possible formation of $CeVO_4$, which may be contributing to the reduction in the corrosion attack, as $CeVO_4$ is solid at the reaction temperature of 900 °C. Wang et al. (Ref 21-24) were the first to introduce rare earth elements to improve wear and corrosion. Initially, research was concentrated on the optimization of the general NiCrAlY composition, i.e., the Ni/Co ratio and the correct allocation of the Cr and Al portions (Ref 25). Later work was carried out to improve the microstructure and corrosive resistance of these coatings by the addition of cerium oxide (Ref 26). There is no reported literature so far on the hot corrosion studies of D-gun sprayed NiCrAlY + 0.4 wt.% $CeO_2$ coating on the superalloys. The present work, therefore, has been focused to investigate the hot corrosion of NiCrAlY + 0.4 wt.% $CeO_2$ coatings deposited on the selected superalloys. Weight change technique has been used to establish the kinetics of hot corrosion of the coated and bare superalloys exposed to molten salt environment, $Na_2SO_4$ and $V_2O_5$ under cyclic conditions at 900 °C. The microstructural characterizations and phase identifications of the coated samples and corrosion products were carried out by FE-SEM/EDAX, x-ray mapping, and x-ray diffraction (XRD), respectively, to elucidate the corrosion mechanisms.

## 2. Experimental Procedure

### 2.1 Development of Coatings

**2.1.1 Samples and Coating Powders.** Nickel- and Iron-based superalloys superni 75, superni 718, and superfer 800H were used as the substrates, which were procured from Mishra Dhatu Nigam Limited, Hyderabad (India) in the rolled sheet form. Nominal compositions of the superalloys substrate materials are shown in Table 1 (Ref 27). Rectangular specimens of dimensions (in mm) $20 \times 15 \times 5$ were cut from the alloy sheets, polished using emery papers of 220, 400, and 600 grit sizes and subsequently on 1/0, 2/0, 3/0, and 4/0 grades. Samples were degreased with acetone and subsequently grit blasted with alumina powders (Grit 45) (36 mesh size) before deposition of the coating by the D-gun process.

A commercially available NiCrAlY (particle size: 5/45 μm, H.C. Starck-413.3) powder with the chemical composition of Ni-22Cr-10Al-1Y was chosen for the deposition of coatings. Figure 1 shows that the particles are of spherical shape with wide particle size distribution, ranging from 5 to 35 μm, which are nearly consistent with the nominal size range provided by the manufacturer. The particle size less than 5 μm depicts the presence of cerium oxide. A mixture of $CeO_2$ (0.4 wt.%) with 99.99% purity and NiCrAlY powder were dry-ball milled in a conventional rotating ball mill with stainless steel balls as a milling/grinding medium for 8 h to obtain the homogenous powder for the deposition of coatings.

**2.1.2 Detonation-Gun Coating.** D-gun process was used to apply coatings on the superalloys at SVX Powder M Surface Engineering Pvt. Ltd, New Delhi (India). Standard spray parameters were used for depositing the NiCrAlY + 0.4 wt.% $CeO_2$ coatings. All the process parameters, including the spray distance, were kept constant throughout the coating process. The spraying parameters were oxygen/acetylene flow rate (ratio) −1:1.21, carrier gas flow rate ($N_2$) −0.82 ($m^3$/h), frequency 3 shots/s, spot size diameter 20 mm, and spraying distance from nozzle to 165 mm. The thickness of the coatings was measured from the optical microscope images, taken along the cross section of the mounted samples. The average thickness of the coatings ranges from 200 to 250 μm.

### 2.2 Characterizations of the Coating

XRD analysis of the coated samples was carried out using a Bruker AXS D-8 Advance Diffractometer (Germany) with Cu $K_\alpha$ radiation and nickel filter at 20 mA under a voltage of 35 kV. The specimens were scanned with a scanning speed of 1 kcps in 2θ range of 10-90° and the intensities were recorded at a chart speed of 1 cm/min with 2°/min as Goniometer speed. The diffractometer interfaced with Bruker DIFFRAC plus XRD software provides *d*-spacing values directly on the diffraction pattern. The samples were wheel cloth polished and then subjected to field emission scanning electron microscope (FEI, Quanta 200F Company) for image acquisition which entailed a backscattered electron image (BSEI) and secondary electron image (SEI) mode. An accelerating voltage of 20-25 kV, a working distance of 9-10 mm, and an image

**Table 1 Chemical composition of the substrate material**

| Alloy Midhani grade (similar grade) | Chemical composition (wt.%) | | | | | | | | | | |
|---|---|---|---|---|---|---|---|---|---|---|---|
| | Fe | Ni | Cr | Ti | Al | Mo | Mn | Si | Cu | Ta | C |
| Superni 75 (Nimonic 75) | 3.0 | 77.1 | 19.5 | 0.3 | | | | | | | 0.1 |
| Superni 718 (Inconel 718) | 18.5 | 52.37 | 19.0 | 0.9 | 0.5 | 3.05 | 0.18 | 0.18 | 0.15 | 5.13 | 0.04 |
| Superfer 800H (Incoloy 800H) | 43.8 | 32.0 | 21.0 | 0.3 | 0.3 | | 1.5 | 1.0 | | | 0.1 |

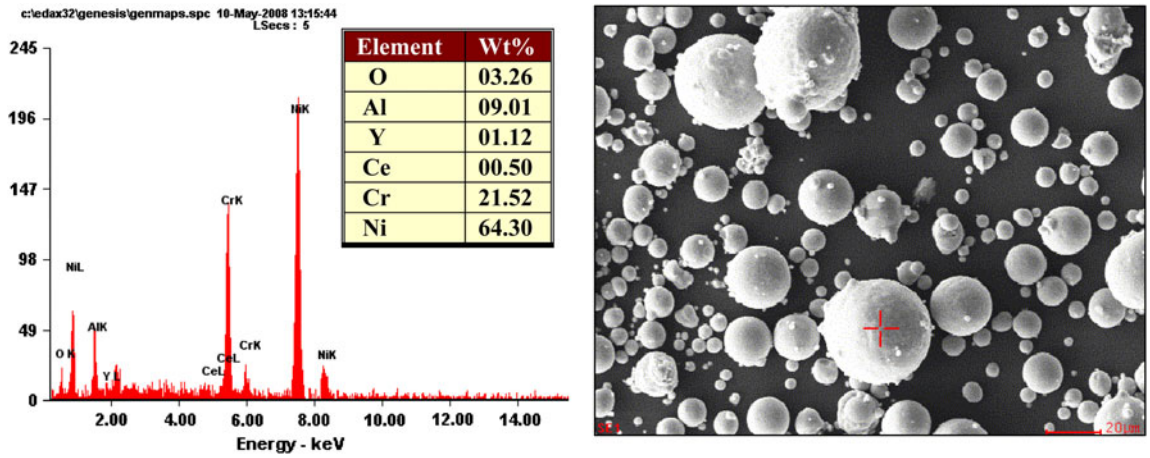


**Fig. 1** SEM of NiCrAlY + 0.4 wt.% $CeO_2$ powder with EDAX elemental composition

size of 1024 * 884 pixels were used for getting quality images for characterizing the surface morphology of the coatings. After preliminary characterization, the samples were cut in cross section, hot mounted in transoptic powder and subjected to mirror polishing, using emery papers of 220, 400, and 600 grit sizes and subsequently on 1/0, 2/0, 3/0, and 4/0 grades, successively. The polished samples were characterized to obtain their cross-sectional morphology and x-ray mapping of the coatings by using FE-SEM/EDAX. The EDAX Genesis software was used to calculate the composition of the elements in the coatings from their corresponding emitted characteristic x-rays.

### 2.3 Hot Corrosion Studies in Molten Salt Environment

Hot corrosion studies were performed in a molten salt (40% $Na_2SO_4$-60% $V_2O_5$) for 100 cycles under cyclic conditions. Each cycle consisted of 1 h heating at 900 °C in a silicon carbide tube furnace followed by 20 min cooling at room temperature (25 °C). The studies were performed for bare as well as coated specimens for comparison. A salt mixture of 40% $Na_2SO_4$-60% $V_2O_5$ was properly prepared in distilled water. After washing with acetone, the specimens were then heated in an oven to about 250 °C. The pre-heating of the specimens was found to be necessary for proper adhesion of the salt layer. Thereafter, a layer of 40% $Na_2SO_4$-60% $V_2O_5$ mixture was applied uniformly on the warm polished specimens with a brush. Amount of the salt coating was kept in the range of 3.0-5.0 mg/cm$^2$. The salt coated specimens as well as the alumina boats were then kept in the oven for 3-4 h at 150 °C. Then they were again weighed before exposing to hot corrosion tests in a laboratory silicon carbide tube furnace. The furnace was calibrated to a variation of ±5 °C. During hot corrosion runs, the weight of boats with specimens were measured together at the end of each cycle with the help of a thermogravimetric balance model 06120 (Contech, India) with a sensitivity of 1 mg. The weight change measurements were made on the sample, adherent oxide on the total sample, and collected spallation. The spalled scale was also included at the time of measurements of weight change to determine total rate of corrosion. The kinetics of corrosion was determined from weight gain plot of weight change/unit area with time. XRD, FE-SEM/EDAX, and x-ray mapping techniques were used to analyze the corrosion products.

## 3. Results

### 3.1 Surface Morphology of the Detonation-Gun As-Sprayed Coatings

FE-SEM micrographs along with EDAX analysis of as-sprayed and polished surface of NiCrAlY + 0.4 wt.% $CeO_2$ coating is shown in Fig. 2(a) and (b). The as-sprayed surface is dense and free of cracks, represents flat glassy melted region and partially melted zones (Fig. 2a). As-sprayed polished coating depicts the formation of nearly globular dendritic structure with Al streaks distributed along the splat boundaries (Fig. 2b).

### 3.2 Weight Change Measurements

The kinetics of hot corrosion were determined from the weight change (mg/cm $^2$) versus time plots for the bare and coated three superalloys subjected to hot corrosion in 40% $Na_2SO_4$-60% $V_2O_5$ environment at 900 °C up to 100 cycles as shown in Fig. 3. The bare superalloy superfer 800H shows a higher weight gain followed by superni 75 as compared with coated one, where as bare superni 718 superalloy has shown a parabolic behavior up to 25 cycles with some spalling/sputtering. With the progress of studies, corrosion products started falling outside the boat, there by it becomes difficult to monitor actual weight gain. The sputtering continued up to 70 cycles thereafter it has ceased. Further, negligible weight gain was noticed up to 100 cycles. The NiCrAlY + 0.4 wt.% $CeO_2$ coated superalloys in all cases show a much lower weight gain than the bare specimens in the given molten salt environment. Coated superfer 800H showed the lowest weight gain, where as bare superfer 800H showed highest weight gain. Whereas among coated superalloys, superni 75 showed highest weight gain followed by superni 718 and superfer 800H, respectively. The weight gain by coated superfer 800H and superni 718 after 100 cycles is nearly 45 and 15% less than that of coated superni 75. It is also found that 60 and 15% saving in overall weight gain for NiCrAlY + 0.4 wt.% $CeO_2$ coated superfer 800H and superni 75 in comparison with the bare superfer 800H and superni 75, respectively. In general, the hot corrosion behavior of both bare and coated samples follow a parabolic rate law, except for bare superfer 800H, as it slightly deviates from parabolic rate, as can be inferred from the square of weight

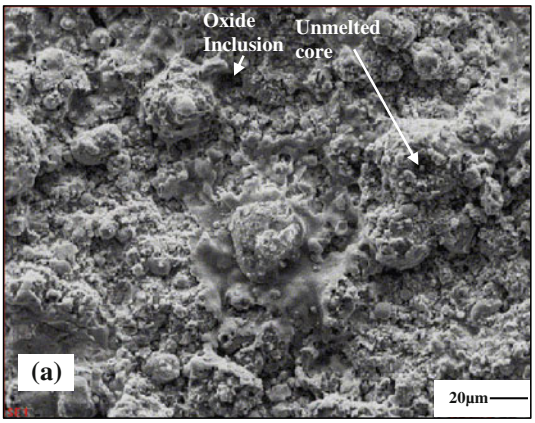


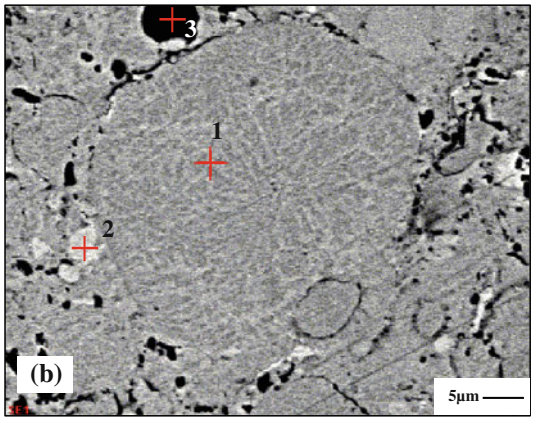


| Elements | Wt% | | |
|---|---|---|---|
| | 1 | 2 | 3 |
| C | **02.75** | **05.91** | **05.02** |
| O | **29.39** | **03.00** | **03.09** |
| Al | **34.19** | **00.00** | **08.17** |
| Ti | **00.61** | **00.42** | **00.50** |
| Ce | **01.74** | **01.20** | **00.97** |
| Cr | **11.62** | **21.46** | **22.35** |
| Fe | **00.50** | **00.07** | **00.42** |
| Ni | **19.19** | **67.93** | **59.47** |
| Y | **00.00** | **00.00** | **00.00** |

**Fig. 2** FE-SEM/EDAX micrographs showing surface morphology of as-sprayed and polished detonation-gun-sprayed NiCrAlY + 0.4 wt.% $CeO_2$ coating on (a) superni 75 and (b) superni 718

change ($mg^2/cm^4$) versus number of cycle plots shown in Fig. 3. Table 2 shows the values of the parabolic rate constants ($K_p$ in $10^{-10}$ $g^2$ $cm^{-4}$ $s^{-1}$) for the NiCrAlY + 0.4 wt.% $CeO_2$ coated and bare superalloys for 100 cycles of hot corrosion. Cumulative weight gain per unit area for coated and bare superalloys is shown in Fig. 4.

### 3.3 X-Ray Diffraction Analysis

The XRD analysis profiles for the scale of D-gun-sprayed NiCrAlY + 0.4 wt.% $CeO_2$ coated superalloy after hot corrosion in 40% $Na_2SO_4$-60% $V_2O_5$ environment for 100 cycles at 900 °C are as illustrated in Fig. 5. The major and minor phases detected on the surface of the specimens with the XRD analysis are CrS, NiO, Ni, $Cr_2O_3$, and $Al_2O_3$, with spinels $NiCr_2O_4$ and $NiAl_2O_3$.

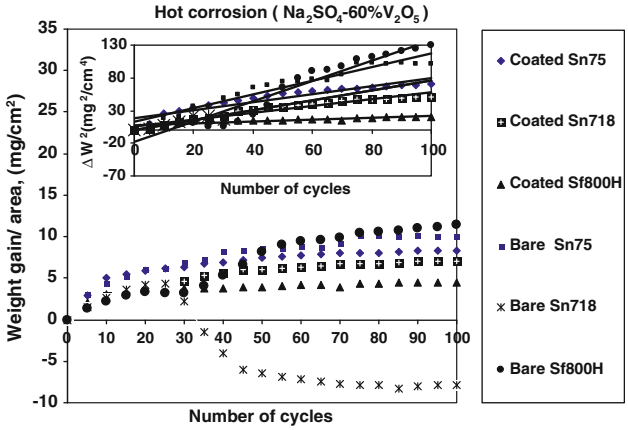


**Fig. 3** Weight gain/area vs. number of cycles plot for NiCrAlY + 0.4 wt.% $CeO_2$ coated and uncoated superalloys subjected to cyclic oxidation for 100 cycles in $Na_2SO_4$-60 wt.% $V_2O_5$ at 900 °C. Inset is fitted for (Weight gain/area)$^2$ vs. number of cycles

**Table 2 Values of the parabolic rate constant, $K_p$**

| Superalloys | Parabolic rate constants ($K_p$), $10^{-10}$ $g^2$ $cm^{-4}$ $s^{-1}$ |
|---|---|
| Bare Superfer 800H | 4.31 |
| Coated Superfer 800H | 0.41 |
| Bare Superni 718 | 2.10 |
| Coated Superni 718 | 1.42 |
| Bare Superni 75 | 2.92 |
| Coated Superni 75 | 1.68 |

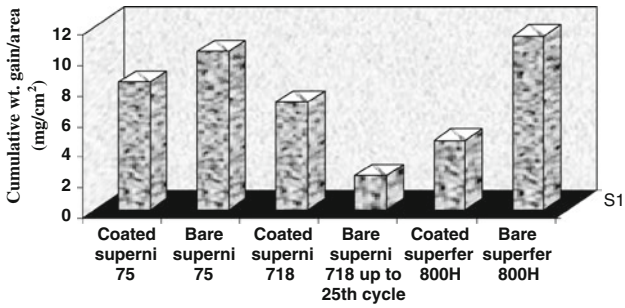


**Fig. 4** Bar chart showing cumulative weight gain per unit area for coated and bare superalloys subjected to cyclic oxidation for 100 cycles in $Na_2SO_4$-60% $V_2O_5$ at 900 °C

### 3.4 FE-SEM/EDAX Analysis of the Scales

**3.4.1 Surface Scale Analysis.** FE-SEM micrographs with EDS spectrum along with EDAX compositional analysis reveals the surface morphology of the NiCrAlY + 0.4 wt.% $CeO_2$ coated substrate superalloy specimens after cyclic hot corrosion in molten salt environment (40% $Na_2SO_4$-60% $V_2O_5$) for 100 cycles at 900 °C are shown in Fig. 6. The surface scale developed on coated superalloys is dense, adherent with few cracks. The corroded coated superalloys showed dense layer on which irregular shaped, white Ni granules are non-uniformly distributed. The EDAX analysis of these white granules shows O and Ni as a principle phase as evident from the high intensity peaks of EDS spectrum (Fig. 6a and c). The other region in the

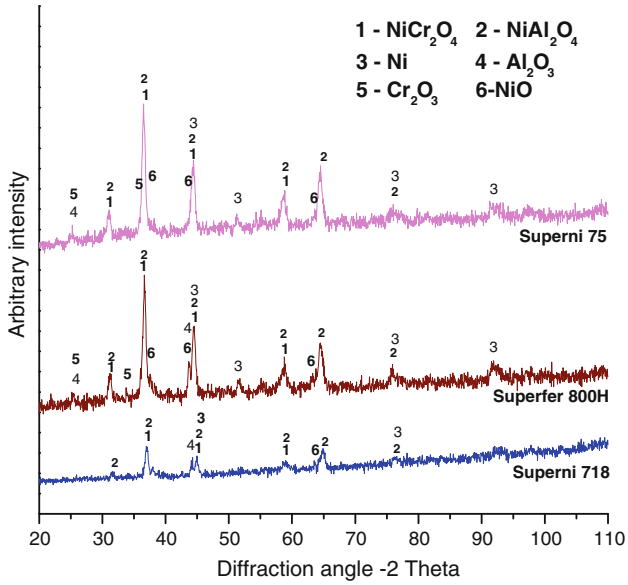


**Fig. 5** X-ray diffraction patterns for NiCrAlY + 0.4 wt.% $CeO_2$ coated superalloys exposed to cyclic oxidation in $Na_2SO_4$-60% $V_2O_5$ environment at 900 °C after 100 cycles

coating is of dark with compact and continuous scale, mainly consisting of O, Al, Cr, and Ni as evident from the high intensity peaks of EDS spectrum with EDAX composition analysis (Fig. 6a, b, and c).

**3.4.2 Cross-Sectional Analysis of the Scale.** Cross-sectional analysis of the scale and the coating was carried out at different points along the cross section of the hot corroded D-gun-coated superni 75, superni 718, and superfer 800H by FE-SEM/EDAX and the results are shown in Fig. 7. All the oxidized NiCrAlY + 0.4 wt.% $CeO_2$ coating on all superalloys show the formation of thin compact, adherent, and continuous oxide scale (nearly 20-μm thick) clearly visible along the cross section of the coating. EDAX analysis of corroded coated superni 75 reveals (Fig. 7a) that the uppermost part of the scale has relatively higher concentration of oxygen along with Ni, Cr, and Al (point 1 and 2), suggesting the formation of oxides of Ni, Cr, and Al. EDAX analysis at point 3 and 5 reveals Ni-rich splats, which remain in un-oxidized state due to absence of oxygen at these points. Oxygen is found at point 4, which indicates the presence of oxides of Al, non-uniformly distributed in the form of streaks. At point 6 (Fig. 7a), a thick band of Cr is found along the coating-substrate interface and the basic elements of the substrate are shown at point 7. Corroded NiCrAlY + 0.4 wt.% $CeO_2$ coated superni 718 (Fig. 7b) showed the top surface of the coating mostly consisting of a homogeneous, adherent and non-uniform oxide scale with variable thickness, the oxide scale mainly consists of Ni, Cr, and Mo (point 1). The white areas (points 2, 4, 5, and 6) in the coating are found to be Ni-rich splats and absence of oxygen at these points suggests that these Ni-rich splats are in the un-oxidized state. The existence of significant quantity of oxygen at black contrast spot (27.83 wt.% at point 3) along with Al and Y depicts the formation of $Al_2O_3$ and $Y_2O_3$. The oxide scale formed on the surface of corroded superfer 800H depicts compact, adherent, and uniform. Existence of higher amount of oxygen on the top surface of the scale (point 1) contains mainly oxides of Ni, Cr, and Al, whereas in the sub-scale region (points 2, 3, and 5) is identified as un-oxidized

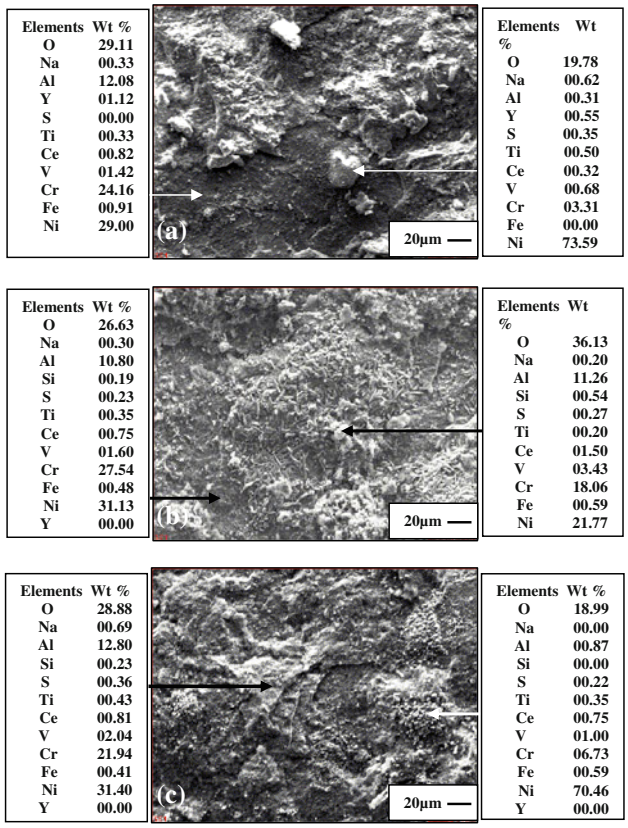


**Fig. 6** FE-SEM/EDAX analysis along with EDS spectrum for coated superalloys subjected to cyclic oxidation in $Na_2SO_4$-60% $V_2O_5$ environment at 900 °C after 100 cycles: (a) superni 75, (b) superni 718, and (c) superfer 800 H

Ni-rich splats which are uniformly spread in the coating. Dark area along the splat boundary (point 4) represents higher amount of oxygen thereby suggesting the oxides of Cr, Ni, and Al. Along the coating-substrate interface (at point 6), concentration of Cr increases significantly with depleted Ni, thereby suggesting the segregation of coating substrate elements.

**3.4.3 X-ray Mapping.** D-gun-sprayed NiCrAlY + 0.4 wt.% $CeO_2$ coated three superalloy samples after hot corrosion in molten salt environment (40% $Na_2SO_4$-60% $V_2O_5$) for 100 cycles at 900 °C were cut across the cross section and mounted in transoptic hot mounting resin. They were mirror-polished and silver pasted between samples and the stub in order to have conductivity, there after, gold coated to facilitate x-ray mapping by FE-SEM/EDS of the different elements present across the scale (Fig. 8-10). FE-SEM/EDS and SEI x-ray mapping of hot corroded coated superni 75 (Fig. 8) showed a very thin oxide scale (10-15 μm) mainly consisting of chromium in the top scale and Ni-rich splats at sub-scale region which partially got oxidized as evident from the oxygen distribution.

Al restricted below the Cr oxide layer. The presence of Fe in the top scale as well as along the splat boundaries in the coating indicates that the Fe might have diffused from the substrate to the top layer of the coating during hot corrosion run. Cerium oxide uniformly distributed along the Ni-rich splat boundaries further it diffused into the substrate (Fig. 8). Vanadium restricted to the top surface of the oxide scale. X-ray mappings for hot corroded NiCrAlY + 0.4 wt.% $CeO_2$ coated superni

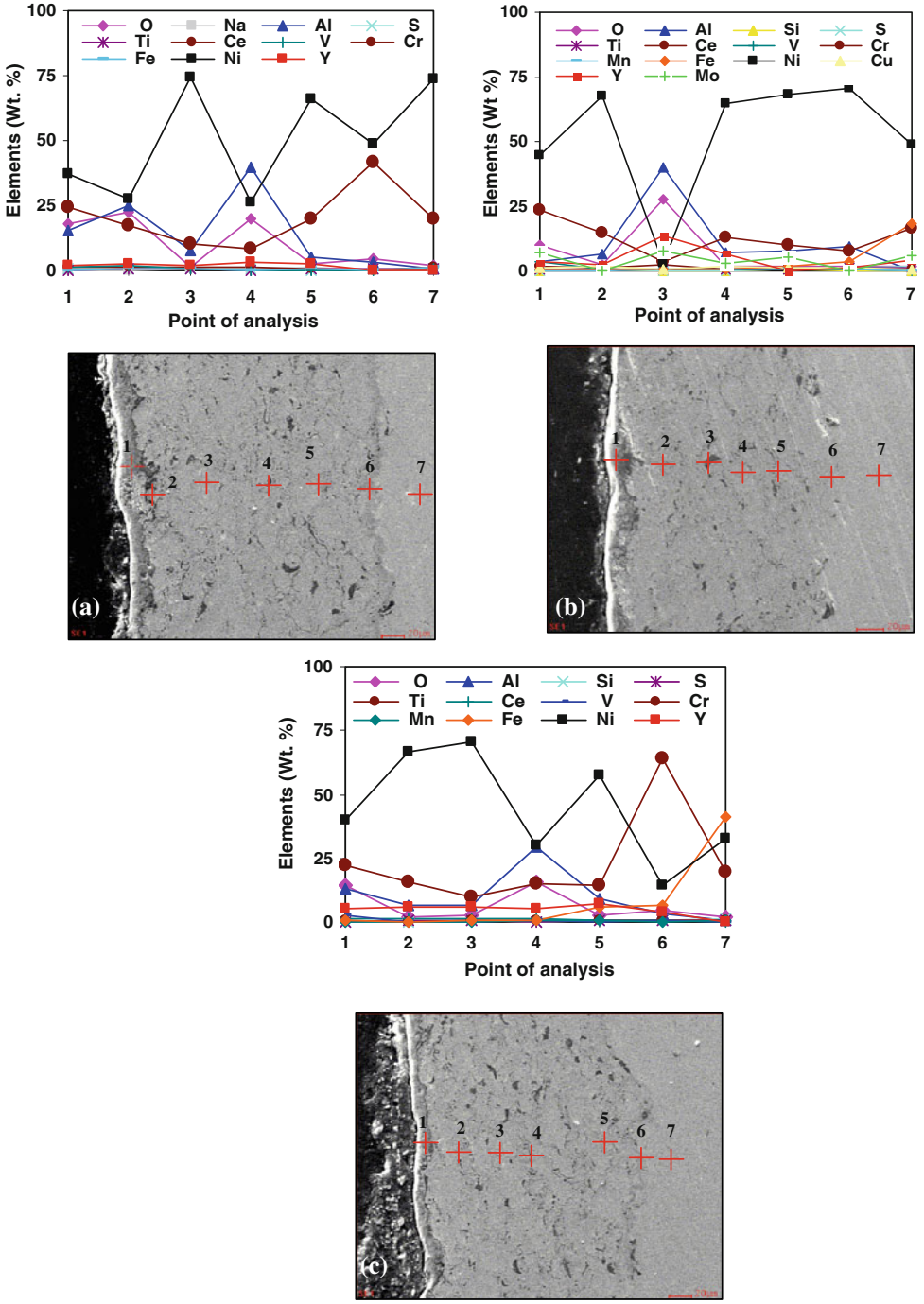


**Fig. 7** Oxide scale morphology and variation of elemental composition across the cross-section of NiCrAlY + 0.4 wt.% $CeO_2$ coated superalloys subjected to cyclic oxidation at 900 °C in molten salt after 100 cycles: (a) superni 75, (b) superni 718, and (c) superfer 800H

718 after 100 cycles at 900 °C (Fig. 9) indicates a variation in the thickness of oxide scale. The top surface mainly consists of chromium along with small amount of Fe and Si, which might have diffused into the coating from the substrate. The sub-scale region is covered with Al and some traces of Al streaks are distributed along the Ni-rich splat boundaries. Similarly, x-ray mapping along the cross-section of the corroded coated superfer 800H sample exposed to 40% $Na_2SO_4$-60% $V_2O_5$ at 900 °C indicates the presence of chromium-rich top scale with a thick band of silicon and iron. Aluminum is distributed in the subscale region and some traces of sulfur are penetrated along the coating-substrate interface. Few streaks of vanadium co-exist with the cerium oxide deep into the coating.

## 4. Discussion

Surface morphology of D-gun-sprayed NiCrAlY + 0.4 wt.% $CeO_2$ coating depicts the presence of oxide inclusion, partial melted powder particles composed of the unmelted cores observed in the regions of the coating surface surrounded by

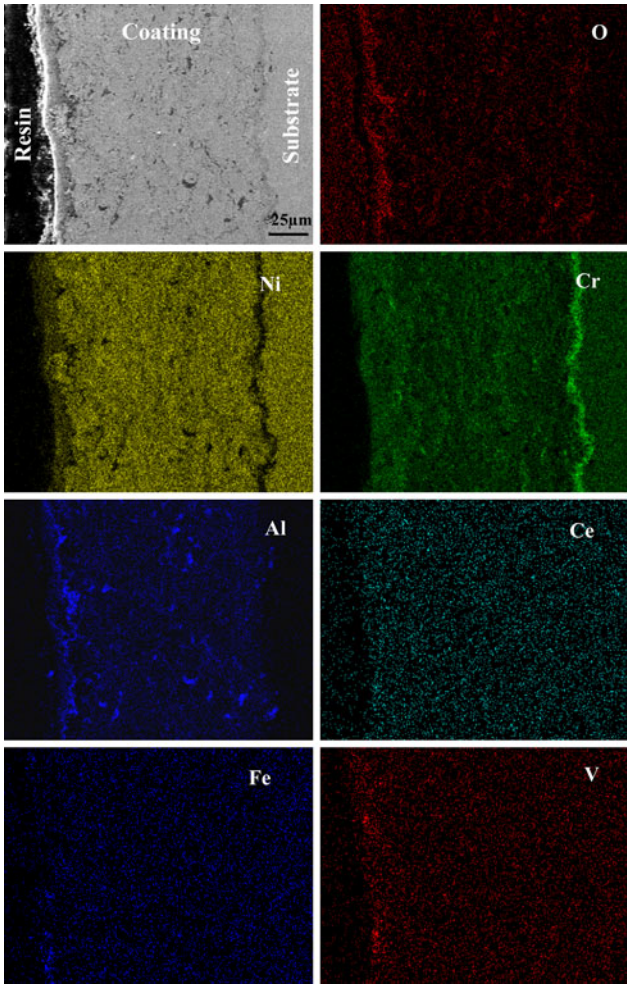


**Fig. 8** Composition image (SE) and x-ray mapping of the cross-section of the NiCrAlY + 0.4 wt.% $CeO_2$ coated superalloy superni 75 subjected to cyclic oxidation at 900 °C in $Na_2SO_4$-60% $V_2O_5$ after 100 cycles

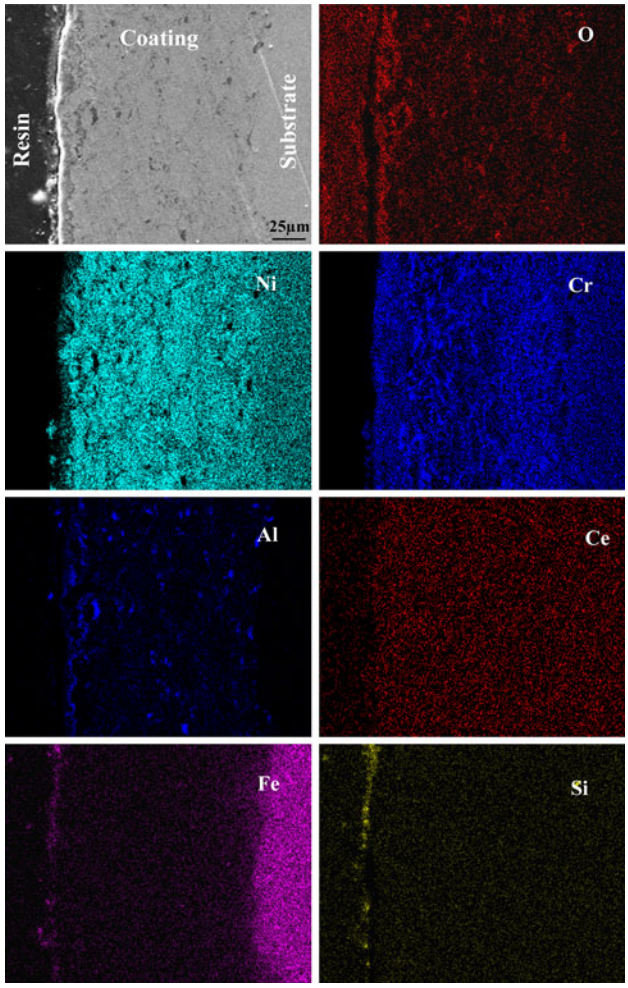


**Fig. 9** Composition image (SE) and x-ray mapping of the cross-section of the NiCrAlY + 0.4 wt.% $CeO_2$ coated superalloy superni 718 subjected to cyclic oxidation at 900 °C in $Na_2SO_4$-60% $V_2O_5$ after 100 cycles

splat debris. The rest of the surface is composed of flat, glassy regions which have arisen as a result of the rapid solidification of molten powder particle after striking the surface. Few micro-pores were observed on the sample surface (Fig. 2a). The polished surface at higher magnification show the formation of globular dendritic structure composed of main elements of coating powder as evident from the EDS elemental composition at point 1 in Fig. 2(b). Due to discontinuous powder flow in the D-gun process, it was observed that such areas with dendritic structure in D-gun coating were larger in size. D-gun coatings are more prone to form dendritic structure (Fig. 2b). The diameter of the dendrite (Fig. 2b) is equal to that of original powder particles (Fig. 1). The particles are not fully melted during spraying; as a result, more unmelted dendritic particles appeared in the coating (Ref 28). Ni and Cr randomly segregated in the form of white patches in the coating as evident from elemental composition (at point 2 in Fig. 2b). High intensity EDS peaks of O and Al show the formation of oxide of Al streaks (point 3 in Fig. 2b), distributed non-uniformly in the coating along the splat boundaries, which is further confirmed by XRD analysis. Zhang et al. (Ref 28) and Chen et al. (Ref 29) had observed similar Al streaks in their studies on air-plasma-sprayed and D-gun sprayed NiCrAlY coating, respectively. The weight gain graph, Fig. 3, shows that the weight gained by bare superalloys increases continuously due to accelerated oxidation in the molten salt environment, where as the coated superalloys in all cases showed better hot corrosion resistance. The bare and coated Fe-based superfer 800H superalloy showed least and highest resistance to the hot corrosion, respectively. The continuous increase in weight of bare superalloys can be attributed to the formation of $NaVO_3$, at a temperature of 900 °C, the $Na_2SO_4$-60% $V_2O_5$ will combine and form $NaVO_3$ having a melting point of 610 °C as reported by Sidhu et al. (Ref 30)

$$Na_2SO_4 + 60\%V_2O_5 = 2NaVO_3 + SO_2 + 1/2O_2 \qquad \text{(Eq 3)}$$

The formation of low melting sodium vanadate causes to dissolve protective oxide scale (Ref 31) as per the following reaction suggested by Sierstein and Kofstad (Ref 32) and Swaminathan et al. (Ref 33)

$$Cr_2O_3 + 4NaVO_3 + 3/2O_2 = 2Na_2CrO_4(l) + 2V_2O_5 \qquad \text{(Eq 4)}$$

Fryburg et al. (Ref 34) and Guo et al. (Ref 35) have suggested that this $Na_2CrO_4$ gets evaporated as a gas. The

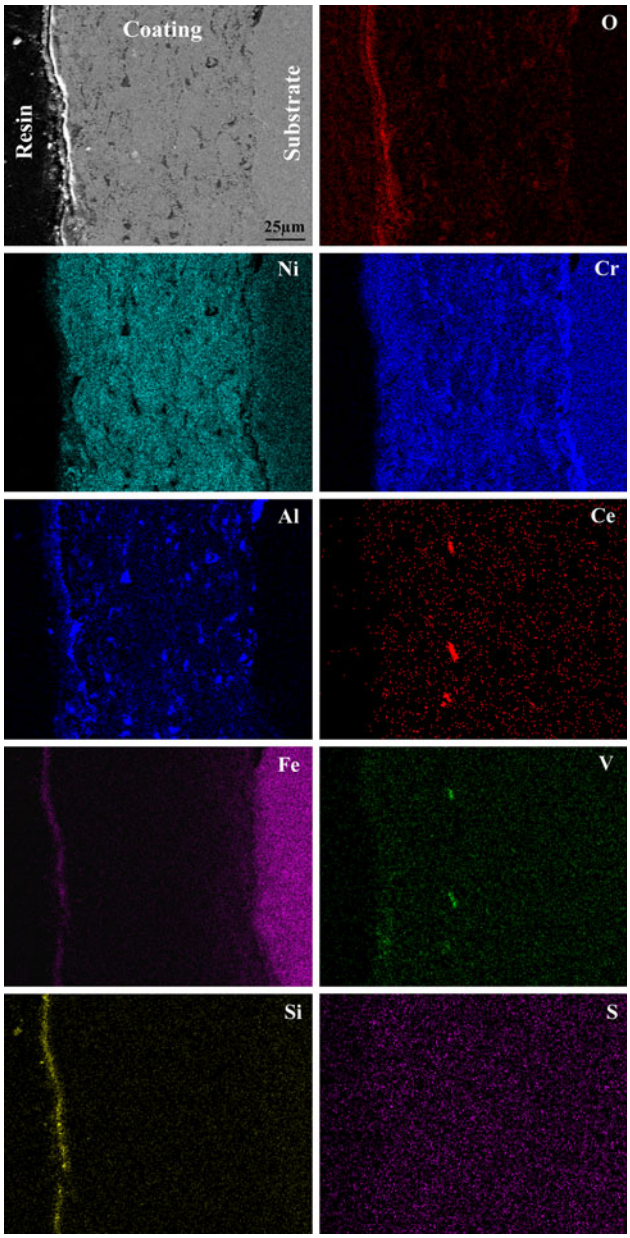


**Fig. 10** Composition image (SE) and x-ray mapping of the cross-section of the NiCrAlY + 0.4 wt.% $CeO_2$ coated superalloy superfer 800H subjected to cyclic oxidation at 900 °C in $Na_2SO_4$-60% $V_2O_5$ after 100 cycles

weight gain of the coated and uncoated specimens is relatively high during the early cycles of hot corrosion, but subsequently increase in weight gain is found to be gradual. Protective oxide of Al has not formed, because Ni and Cr on the surface were oxidized at a faster rate. As the oxidation cycle proceeds, the air entrapped during D-gun deposition and sheltered in the porosities, since the cooling of coating was rapid. There is shortage of time for the residual air to react with the surrounding coating alloys. However, the coating took in situ reaction during high temperature (900 °C) oxidation and formed alumina ($Al_2O_3$) at the splat boundaries and within open pores. During subsequent cycles the formation of oxides has blocked the pores, splat boundaries and acted as diffusion barrier to the inward diffusion of corrosive species. This leads to slow oxide scale growth. All the coated superalloys followed parabolic behavior where as bare superalloys deviates from the parabolic rate law except bare superni 75. Parabolic rate constant for the bare and coated superalloys are shown in Table 2. The overall weight gain of 8.37, 7.077, and 4.53 mg/cm$^2$ was observed for the NiCrAlY + 0.4 wt.% $CeO_2$ coated superni 75, superni 718, and superfer 800H superalloys (Fig. 4), respectively. The NiCrAlY + 0.4 wt.% $CeO_2$ coating provides maximum hot corrosion resistance to superfer 800H and has been found successful in reducing the weight gain by about 60% of that gained without a coating, which further evident from the parabolic rate constant ($K_p = 0.41310^{-10}$ g$^2$ cm$^{-4}$ s$^{-1}$). Coatings on superni 75 reduce the weight gain by 17% that gained by the uncoated superalloys. The comparatively less corrosion resistance shown by coated superni 75 and 718 in comparison with the coated superfer 800H might be due to the presence less protective bigger and more quantity of oxides (NiO) are formed on the surface scale (Fig. 6a and b), which allows the penetration of corrosive species through the scale to the coating. This NiO formed in the surface scale is porous due to re-precipitation by fluxing action; also the scale formed on the surface is non-uniform (Fig. 8a and b) due to which the oxygen has penetrated little deep into the coating as attributed from the x-ray mapping analysis (Fig. 8, 9).

Better performance of coated superfer 800H might be due to uniform, dense, thick scale formed on the surface mainly consisting of Cr, Ni, and Al, presence of these elements along with oxygen represents the formation of oxides of Cr, Ni, Al, and the spinels of $NiCr_2O_4$ and $NiAl_2O_4$ as revealed by XRD analysis (Fig. 5). Presence of $CeO_2$ with vanadium across the coating depicts the formation of $CeVO_4$, which might have further contributed in reducing hot corrosion attack (Fig. 10). The spinel phase usually has lower diffusion coefficients of the cations and anions than those in their parent oxides (Ref 36), the presence of these phases in the scale of coated superalloys is further supported by the surface (Fig. 6c), cross-sectional EDAX (Fig. 7c) and x-ray mapping analyses (Fig. 10). Singh (Ref 37), Wu et al. (Ref 38, 39) reported the formation of similar phases. Further the coating also revealed the formation of continuous thin oxide scale of Si and Fe on the top surface of coated superfer 800H (Fig. 9). These elements have diffused into the coating through the splat boundaries and open pores, which acts as a channel for the transport of coating and substrate elements during initial cycles of hot corrosion, which further contributed to increases the resistance to hot corrosion (Fig. 11). Wang et al. (Ref 40) and Grunling and Bauer (Ref 41) reported that presence of silicon can promote the formation of continuous dense scale and improve the adherence of the outer scale to the coating in the subsequent hot corrosion process. However, Yttrium was found to be segregated along the grain boundaries of $A1_2O_3$ and lowers the scale growth rates (Ref 42, 43). RE segregate to oxide grain boundaries, where they can significantly reduce the outward transport of Al, hence decrease the rate of oxidation and contributed to the improved scale adherence and reduced interfacial void formation (Ref 44). Schematic diagram showing proposed hot corrosion mechanism of the NiCrAlY + 0.4 wt.% $CeO_2$ coated superalloy superfer 800H at 900 °C in $Na_2SO_4$ + 60% $V_2O_5$ after 100 cycles is shown in Fig. 11.

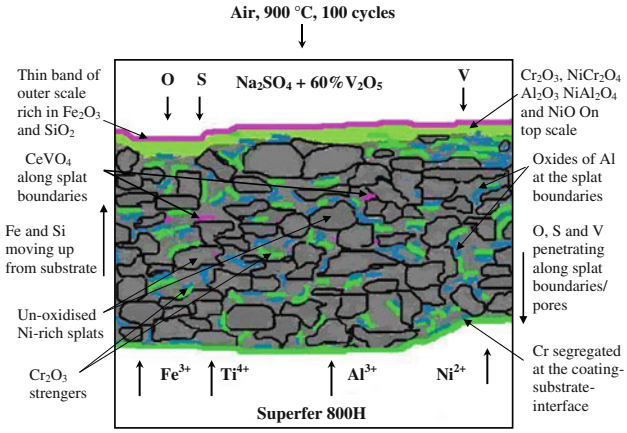


**Fig. 11** Schematic diagram showing proposed hot corrosion mechanism of the NiCrAlY + 0.4 wt.%$CeO_2$ coated superalloy superfer 800H at 900 °C in $Na_2SO_4$ + 60% $V_2O_5$ after 100 cycles

## 5. Conclusions

NiCrAlY + 0.4 wt.% $CeO_2$ coating on Ni- and Fe-based superalloy substrates has been successfully deposited by D-gun spraying process in the present work and the following conclusions are made.

- Surface morphology of the as-sprayed coating depicts the formation of unmelted particles in the form of globular dendritic structure. The diameter of dendritic structure equals to that of original powder particles.
- Cerium oxide is uniformly distributed along the Ni-rich splat boundaries. Traces of Al are distributed along the Ni-rich splat boundaries.
- The bare and coated Fe-based superfer 800H superalloy showed least and highest resistance to the hot corrosion, respectively.
- D-gun-sprayed NiCrAlY + 0.4 wt.% $CeO_2$ coating found to be effective in imparting hot corrosion resistance to superfer 800H in the molten salt environment.
- The formation of oxides along the splat boundaries and within open pores of the coatings might have acted as diffusion barrier to the inward diffusion of molten salt.
- There is 60 and 15% saving in overall weight gain for NiCrAlY + 0.4 wt.% $CeO_2$ coated superfer 800H and superni 75 in comparison with the bare superfer 800H and superni 75, respectively.
- A dense oxide scale formed on the coated superalloys and hot corrosion resistance of coating might be due to the formation of protective phases like NiO, $Cr_2O_3$, $Al_2O_3$, $NiCr_2O_4$, and Ni $Al_2O_4$.
- Formation of small amounts of oxides of iron and silicon show diffusion from the substrate to the top surface of coating.


### Acknowledgments

The authors are very thankful to SVX Powder M Surface Engineering Pvt Ltd, New Delhi (India) for having provided a D-gun coating facility.


### References


1. N.B. Maledi, J.H. Potgieter, M. Sephton, L.A. Cornish, L. Chown, R. Suss, Hot Corrosion Behaviour of Pt-Alloys for Application in the Next Generation of Gas Turbines, International Platinum Conference 'Platinum Surges Ahead', The Southern African Institute of Mining and Metallurgy, 2006, p 81
2. D. Bettge, W. Osterle, and J. Ziebs, Temperature Dependence of Yield Strength and Elongation of the Nickel-Base Superalloy IN738LC and the Corresponding Microstructural Evolution, *Zeitschr. Metalkd.*, 1995, **86**(3), p 190–197
3. S. Esmaeili, C.C. Engler-Pinto, Jr., B. Ilschner, and F. Rezai-Aria, Interaction Between Oxidation and Thermo-Mechanical Fatigue in IN738LC Superalloy, *Scr. Metall. Mater.*, 1995, **33**(11), p 1777–1781
4. M.R. Khajavi and M.H. Shariat, Failure of First Stage Gas Turbine Blades, *Eng. Fail. Anal.*, 2004, **11**, p 589–597
5. G.J. Santoro, F.J. Kohl, C.A. Stems, S.A. Gokoglu, and D.E. Rosner, Experimental and Theoretical Deposition Rates From Salt-Seeded Combustion Gases of a Mach 0.3 Burner Rig, NASA Technical Paper 2225, 1984
6. M.A. DeCrescente and N.S. Bornstein, Formation and Reactivity Thermodynamics of Sodium Sulfate with Gas Turbine Alloys, *Corrosion*, 1968, **24**, p 127–133
7. T.S. Sidhu, Ph.D. Thesis, Metals and Material Engineering Department, Indian Institute of Technology Roorkee, Roorkee, 2006
8. M. Li, X. Sun, W. Hu, and H. Guan, Microstructural Changes and Elemental Diffusion of Sputtered NiCrAlY Coating on a Ni-Base SC Superalloy Subjected to High Temperature, *Mater. Lett.*, 2007, **61**, p 5169–5172
9. S. Kamal, R. Jayaganthan, S. Prakash, and S. Kumar, Hot Corrosion Behavior of Detonation Gun Sprayed $Cr_3C_2$-NiCr Coatings on Ni and Fe-Based Superalloys in $Na_2SO_4$-60% $V_2O_5$ Environment at 900°C, *J. Alloys Compds.*, 2008, **463**, p 358–372
10. S. Kamal, R. Jayaganthan, and S. Prakash, High Temperature Oxidation Studies of Detonation-Gun-Sprayed $Cr_3C_2$-NiCr Coating on Fe- and Ni-Based Superalloys in air Under Cyclic Condition at 900°C, *J. Alloys Compds.*, 2009, **472**(1–2), p 378–389
11. Y.J. Zhang, X.F. Sun, H.-R. Guan, and Z.-Q. Hu, 1050°C Isothermal Oxidation Behavior of Detonation Gun Sprayed NiCrAlY Coating, *Surf. Coat. Technol.*, 2002, **161**, p 302–305
12. Y.J. Zhang, X.F. Sun, Y.C. Zhang, T. Jin, C.G. Deng, H.R. Guan, and Z.Q. Hua, A Comparative Study of DS NiCrAlY Coating and LPPS NiCrAlY Coating, *Mater. Sci. Eng. A.*, 2003, **360**, p 65–69
13. N. Eliaz, G. Shemesh, and R.M. Latanision, Hot Corrosion in Gas Turbine Components, *Eng. Fail. Anal.*, 2002, **9**, p 31–43
14. B. Rajasekaran, S. Ganesh Sundara Raman, S.V. Joshi, and G. Sundararajan, Effect of Detonation Gun Sprayed Cu-Ni-In Coating on Plain Fatigue and Fretting Fatigue Behaviour of Al-Mg-Si Alloy, *Surf. Coat. Technol.*, 2006, **201**, p 1548–1558
15. R. Venkataraman, B. Ravikumar, R. Krishnamurthy, and D.K. Das, A Study on Phase Stability Observed in as Sprayed Alumina-13 wt% Titania Coatings Grown by Detonation Gun and Plasma Spraying on Low Alloy Steel Substrates, *Surf. Coat. Technol.*, 2006, **201**, p 3087–3095
16. Y.S. Tian, C.Z. Chen, L.X. Chen, and Q.H. Huo, Effect of RE Oxides on the Microstructure of the Coatings Fabricated on Titanium Alloys by Laser Alloying Technique, *Scr. Mater.*, 2006, **54**, p 847–852
17. T. Zhang and D.Y. Li, Effects of Cerium on Dry Sand Erosion and Corrosive Erosion of Aluminide Coating on 1030 Steel, *J. Mater. Sci. Lett.*, 2000, **19**, p 429–432
18. T. Zhang and D.Y. Li, Effects of Yttrium on Corrosive Erosion and Dry Sand Erosion of FeAlCr (Y) Diffusion Coatings on 1030 Steel, *Mater. Sci. Eng. A*, 2000, **277**, p 18–24
19. A.U. Seybolt, Role of Rare Earth Additions in the Phenomenon of Hot Corrosion, *Corr. Sci.*, 1971, **1**, p 751–761
20. Gitanjaly, Ph.D. Thesis, Metals and Material Engineering Department, IIT, Roorkee, India, 2003
21. Y. Wang, Z.H. Yu, J.J. Liu, C.S. Wang, and Q.A. Li, The Influence of $CeO_2$ on the Microstructure and Wear Resistance of M80S20 Flame Spray and Flame Spray Welding Coatings, *J. Rare Earths*, 1992, **10**, p 212–216
22. Y. Wang, J.J. Liu, and Z.H. Yu, Effect of Rare Earth Elements on Microstructure and Wear Resistance of Laser Remelted Iron Alloy Coatings Containing Metalloids, *Surf. Eng.*, 1993, **9**, p 151–153

23. Y. Wang, J. Liu, and R. Kovacevic, Mechanism of Surface Modification of CeO in Laser Remelted Alloy Spray Coatings, *Wear*, 1998, **221**, p 47–53
24. Y. Wang, W. Chen, and L. Wang, Micro-Indentation and Erosion Properties of Thermal Sprayed NiAl Intermetallic-Based Alloy Coatings, *Wear*, 2003, **254**, p 350–355
25. N. Czech, F. Schmitz, and W. Stamm, Improvement of MCrA1Y Coatings by Addition of Rhenium, *Surf. Coat. Technol.*, 1994, **68/69**, p 17–21
26. J.F. Li and C.X. Ding, Polishing-Induced Pull Outs of Plasma Sprayed $Cr_3C_2$-NiCr Coating, *J. Mater. Sci. Lett.*, 1999, **18**, p 1719–1721
27. S. Kamal, R. Jayaganthan, and S. Prakash, Characterisation of Detonation Gun Sprayed $Cr_3C_2$ 25% NiCr Coatings on Ni- and Fe-Based Superalloys, *Surf. Eng.*, 2009, **25**(4), p 287–294
28. Y.J. Zhang, X.F. Sun, Y.C. Zhang, T. Jin, C.G. Deng, H.R. Guana, and Z.Q. Hua, A Comparative Study of DS NiCrAlY Coating and LPPS NiCrAlY, *Coat. Mater. Sci. Eng. A*, 2003, **360**, p 65–69
29. W.R. Chen, X. Wu, B.R. Marple, and P.C. Patnaik, Oxidation and Crack Nucleation/Growth in an Air-Plasma-Sprayed Thermal Barrier Coating with NiCrAlY Bond Coat, *Surf. Coat. Technol.*, 2005, **197**, p 109–115
30. T.S. Sidhu, S. Prakash, and R.D. Agrawal, Hot Corrosion Behaviour of HVOF-Sprayed NiCrBSi Coatings on Ni and Fe-Based Superalloys in $Na_2SO$-60% $V_2O_5$ Environment at 900°C, *Acta Mater.*, 2006, **54**, p 773–784
31. I. Gurrappa, Identification of Hot Corrosion Resistant MCrAlY Based Bond Coatings for Gas Turbine Engine, *Appl. Surf. Coat. Technol.*, 2001, **139**, p 272–283
32. M. Seiersten and P. Kofstad, The Effect of $SO_3$ on Vanadate-Induced Hot Corrosion, *High Temp. Technol.*, 1987, **5**(3), p 115–122
33. J. Swaminathan, S. Raghavan, and S.R. Iyer, Studies on the Hot Corrosion of Some Nickel-Base Superalloys by Vanadium Pentoxide, *Trans. Indian Inst. Met.*, 1993, **46**(3), p 175–181
34. G.C. Fryburg, F.J. Kohl, and C.A. Stearns, Chemical Reactions Involved in the Initiation of Hot Corrosion of IN-738, *J. Electrochem. Soc.*, 1984, **131**(12), p 2985–2997
35. M.H. Guo, Q.M. Wang, P.L. Ke, J. Gong, C. Sun, R.F. Huang, and L.S. Wen, The Preparation and Hot Corrosion Resistance of Gradient NiCoCrAlYSiB Coatings, *Surf. Coat. Technol.*, 2006, **200**, p 3942–3949
36. U.K. Chatterjee, S.K. Bose, and S.K. Roy, *Environmental Degradation of Metals*, Marcel Dekker, New York, 2001
37. B. Sidhu, Ph.D. Thesis, Metals and Material Engineering Department, Indian Institute of Technology Roorkee, Roorkee, 2003
38. Y.N. Wu, G. Zhang, Z.C. Feng, B.C. Zhang, Y. Liang, and F.J. Liu, Oxidation Behavior of Laser Remelted Plasma Sprayed NiCrAlY and NiCrAlY-$Al_2O_3$ coatings, *Surf. Coat. Technol.*, 2001, **138**, p 56–60
39. X. Wu, D. Weng, Z. Chen, and L. Xu, Effects of Plasma-Sprayed NiCrAl/$ZrO_2$ Intermediate on the Combination Ability of Coatings, *Surf. Coat. Technol.*, 2002, **140**, p 231–237
40. Q.M. Wang, Y.N. Wu, P.L. Ke, H.T. Cao, J. Gong, C. Sun, and L.S. Wen, Hot Corrosion Behavior of AIP NiCoCrAlY(SiB) Coatings on Nickel Base Superalloys, *Surf. Coat. Technol.*, 2004, **86**, p 389–397
41. H.W. Grunling and R. Bauer, The Role of Silicon in Corrosion-Resistant High Temperature Coatings, *Thin Solid Films*, 1982, **95**, p 3–20
42. G.W. Goward, Progress in Coatings for Gas Turbine Airfoils, *Surf. Coat. Technol.*, 1998, **108–109**, p 73–79
43. H.M. Tawancy and N. Sridhar, High-Temperature Oxidation Behavior of Ni-Cr-AI-Fe-Y Alloy, *Oxid. Met.*, 1992, **37**(3/4), p 143–166
44. B.A. Pint, Experimental Observations in Support of the Dynamic-Segregation Theory to Explain the Reactive-Element, *Effect Oxidation of Metals*, 1996, **45**, p 1–37